Investigation of the composition and structure of GP zones in Al - Ag by means of positron annihilation

1996 J. Phys.: Condens. Matter 8 7523

(http://iopscience.iop.org/0953-8984/8/40/015)

J. Phys.: Condens. Matter **8** (1996) 7523–7537. Printed in the UK

Investigation of the composition and structure of GP zones in Al–Ag by means of positron annihilation

G Bischof†, V Gröger†, G Krexner‡ and R M Nieminen§

† Institute of Solid State Physics, University of Vienna, Strudlhofgasse 4, A-1090 Wien, Austria

‡ Institute of Experimental Physics, University of Vienna, Strudlhofgasse 4, A-1090 Wien, Austria

§ Laboratory of Physics, Helsinki University of Technology 02150 Espoo, Finland

Received 14 March 1996, in final form 29 May 1996

Abstract. Positron annihilation spectroscopy is used to obtain information about structures and concentrations of η- and ε-GP zones in Al–Ag alloys. Measurements of positron lifetimes and Doppler broadening are reported. For the interpretation we present a method to estimate numerically the lifetimes of positrons trapped in spherical precipitates and give results for a series of possible concentrations and internal structures of the precipitated particles. From a comparison with the experimental data we conclude that the silver atoms are distributed homogeneously inside the ε-GP zones and that the silver concentration of both types of zone is 60 ± 5 at.%.

1. Introduction

Al–Ag is a useful model system for the case of alloys consisting of atoms of similar radii (difference $\approx 0.5\%$) with nearly negligible elastic interactions. Therefore the driving force for the creation and coarsening of precipitates must be for the most part of electronic origin. Moreover it has the advantage that due to the large difference between the atomic numbers of aluminium and silver many experimental techniques (such as small-angle x-ray scattering (SAXS), transmission electron microscopy (TEM), and positron annihilation spectroscopy (PAS)) are expected to exhibit a strong contrast between precipitates and the matrix.

For an alloy quenched from the α-region of the phase diagram (figure 1), the decomposition starts by the formation of nearly spherical silver-rich preprecipitates (GP zones) with the fcc structure. For later stages the platelike metastable γ'-precipitates with the hexagonal close-packed (hcp) structure develop. Finally, the stable hcp γ-phase (Ag_2Al) evolves.

Various aspects related to the composition, structure and shape of the GP zones are still subject to discussion. In particular, the existence of two types of GP zone has been presumed, so called η-zones below about 170 °C and ε-zones at higher temperatures. Starting from the assumption that the Ag concentrations are about 60 at.% for the η-zones and 30 at.% for the ε-zones a metastable miscibility gap of unusual shape with a shoulder below 170 °C has been proposed. In figure 1 this miscibility gap is illustrated. Köster *et al* [1] reported from experimental results for electrical conductivity and hardness that the transition between the two phases is reversible.

0953-8984/96/407523+15$19.50

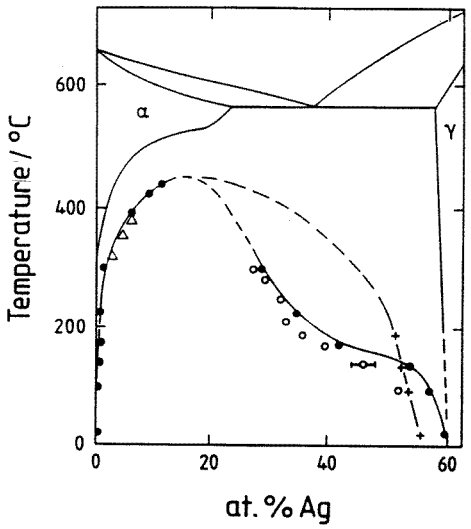

Figure 1. The equilibrium phase diagram of Al–Ag with the metastable miscibility gap as it is currently widely accepted. The conspicuous asymmetry is at variance with the present investigation. Δ, points found by Borelius [26]; ○, points found by Baur and Gerold [2]; ●, points found by Osamura *et al* [3]; +, points found by Naudon and Caisso [8].

Baur and Gerold [2], using SAXS, Osamura *et al* [3], using atom-probe field ion microscopy (AP FIM) and Krause *et al* [4], Bharathi *et al* [5] and Dlubek *et al* [6, 7] using PAS supported the idea of an asymmetric miscibility gap as described above. Naudon and Caisso [8] and Dubey *et al* [9], however, did not observe such a distinct change in the zone composition with aging temperature. But from the presence of two peaks in a Porod representation of SAXS data for the ε-regime, both groups suggested a different silver *distribution* in η- and ε-zones. The η-zones are reported to be homogeneous (possibly short-range ordered [3, 10]), and the ε-zones are claimed to be of a more complex structure: while a silver-enriched core and a depleted shell were suggested by Naudon and Caisso, a depleted core and an outer shell of nearly pure silver were postulated by Dubey *et al* [9].

In a high-resolution electron microscopy (HREM) study Ernst and Haasen [11] could not differentiate between η and ε though their high-resolution lattice imaging is based on mass contrast. Later Al-Kassab and Haasen [12] found by analytical FIM both compositions (35 at.% and 55 at.% Ag) to coexist locally in neighbouring precipitates. Due to the small sample volume of their technique, however, the volume fraction of ε and η could not be determined.

Langmayr *et al* [13] investigated the coarsening of the GP zones at 120 °C and 190 °C with SAXS and could not find any indication of a contraction of the miscibility gap.

In this situation we want to contribute by PAS to the question of the structure of the ε-particles. As positrons are expected to be trapped by silver-enriched particles due to the difference in the positron affinity (see subsection 3.1 and [14]), the possible occurrence of a trapped state, values of defect lifetimes and Doppler broadening parameters will lead to a decision between the various different structures in discussion. This decision can only be made by comparison of the measured PAS data with the results of careful model calculations which are made for all of the structures in consideration.

2. Experimental details

Aluminium of purity 5 N and silver (6 and 1 at.%) of purity 4 N was melted in an induction furnace in argon atmosphere. After rolling to about half of the thickness, the samples were homogenized at 823 K for 4 d. For the positron measurements the samples were rolled to the final thickness of about 1 mm, cut into 8×8 mm^2 squares and again homogenized. Composition and homogeneity were checked by microprobe and by measurements of the electrical resistivity by a four-point method. The samples were then annealed at RT and 150 and 190 °C respectively for times short enough to avoid the presence of concomitant γ'-precipitates [9]. We additionally used a step by step quenching procedure in order to produce large ε-particles. The samples were quenched down from the homogenization temperature to 200 °C, held at this temperature for about 25 s and then quenched into cold water. This procedure has been reported to produce ε-precipitates with radii of 60–70 Å [10].

For PAS measurements, two identical samples were sandwiched with a 3×10^5 Bq ^{22}Na positron source, evaporated onto a 1.14 mg cm^{-2} Kapton foil. The lifetime measurements were carried out at room temperature using a fast–slow coincidence system with a resolution of 220 ps in operating conditions. The spectra, containing at least 5×10^6 counts each, were analysed by the *Resolution* and *Positronfit* computer programs [15, 16]. The Doppler-broadened energy spectrum of the annihilation radiation was also measured for all samples, using a high-purity germanium detector with energy resolution of 1.2 keV and a channel width of 25.9 eV. Eighty central channels out of 600 were used for the determination of the S-parameter [17]. For comparison, we also measured the lifetimes and S-parameters for pure aluminium and silver samples.

Additional information on the average radius of the precipitates is necessary for the complete interpretation of the PAS data. The time development of particle dimensions during annealing at 150 and 190 °C has been investigated by Dubey [18]. We performed SAXS measurements on two samples for comparison. From the intensity distribution the Guinier radius of the GP zones was estimated and from that the geometrical radius. Furthermore, an estimate of the mean zone separation was obtained from the scattering maximum. The investigation of the 6 at.% samples annealed at 150 °C for 40 min gave an average particle radius of 23 Å and an average zone separation of 97 Å. A 2 min annealing at 190 °C gave particle radii of about 20 Å and zone separations of 114 Å. The results are in agreement with the data given by Dubey [18].

In order to make sure that the different kinds of precipitate (η and ε) were actually produced, measurements of the micro-hardness of the samples were performed. It could clearly be shown that two different phases exist. The Vickers micro-hardness (HV) of the Al–6 at.% Ag alloy annealed at 150 °C was about 92 kp mm^{-2}. When the annealing took place at 190 °C the HV decreased to 79 kp mm^{-2}. This process is reversible, and the metastable phase produced at 190 °C (ε-precipitates) survives unchanged over the whole period of a PAS measurement at room temperature.

We performed eight sets of PAS experiments and between each set a calibration measurement was carried out. After source and background corrections, the lifetime spectra could be well fitted with only one component assigned to a positron state trapped at the precipitates. The absence of a bulk component can be understood by the fact that the zone separation ($\approx$ 100 Å) is much smaller than the mean positron diffusion length of about 1000 Å which results in saturated positron trapping by the zones. The results are shown in table 1. For each point we used several paired samples. Due to sample preparation there is a certain spread in the line shape parameter and lifetime results. Therefore we specified

Table 1. Average experimental positron lifetimes and *S*-parameters in Al–Ag alloys with different initial silver concentrations and annealing temperatures.

Sample	Temp. (°C)	Lifetime (ps)	*S*-parameter	S/S_{Al}
Aluminium	—	160 ± 2	0.6247	1
Silver	—	135 ± 2	0.5437	0.8703
6 at.% Ag	RT	140 ± 3	0.5647 ± 0.0005	0.9040
6 at.% Ag	150, 40 min	141 ± 3	0.5630 ± 0.0006	0.9012
6 at.% Ag	190, 2 min	140 ± 3	0.5637 ± 0.0005	0.9024
6 at.% Ag	190, 15 min	142 ± 4	0.5659 ± 0.0005	0.9064
6 at.% Ag	190, 60 min	142 ± 3	0.5657 ± 0.0006	0.9056
1 at.% Ag	150, 15 min	149 ± 3	0.5886 ± 0.0003	0.9422
1 at.% Ag	190, 15 min	149 ± 4	0.5894 ± 0.0024	0.9435
6 at.% Ag	stepwise	143 ± 3	0.5625 ± 0.0022	0.9004
1 at.% Ag	stepwise	143 ± 3	0.5668 ± 0.0022	0.9073

the average value and the maximum deviation observed for each set of measurements (the purely statistical errors are considerably smaller). For both concentrations considered the trapped positron states turn out to be very similar for the different kinds of precipitate. Therefore it will be necessary to carry out model calculations for all possible structures of ε-zones in order to find out which of them is compatible with experiment.

The Al–1 at.% Ag samples were annealed only for a short time to produce small particles with radii of about 10 Å. These values were derived from the results of Dubey [18]. They can be considered to be reliable since there is good agreement between the particle sizes of Dubey and our own SAXS results for the 6 at.% samples. In this way the effects of the particle size on the positron lifetimes could be checked as will be discussed later.

3. Model calculations

The theory accompanying positron annihilation has developed in the last two decades to *first-principles* methods predicting the annihilation characteristics for different environments and conditions. This development has occurred in parallel with the development of electronic structure calculations, which in turn is made possible by the progress in computational techniques. The basis of the modern electronic structure calculations for solids is the density functional theory. It turns out that the *ab initio* determination of positron states in solids is possible on the basis of a two-component generalization of the density functional theory (see for a review [19]).

Though the exact calculation of the annihilation characteristics of localized positrons is possible in principle, the calculational effort explodes with increasing complexity of the positron trap. In fact, it is impossible to simulate GP zones consisting of thousands of atoms on contemporary computers with *first-principles* methods.

In order to make predictions about the positron annihilation in the η- and ε-zones at all, we have developed an approximate method to estimate the positron lifetimes and use them for an analysis of GP zone compositions. The way we proceed is as follows. First the positron affinities and positron annihilation rates in bulk Al–Ag alloys of different homogeneous silver concentrations are calculated. Then the different possible structures of the GP zones are simulated by spherical well models in order to estimate the positron annihilation characteristics of these precipitates.

3.1. Positron affinities and annihilation rates in Al–Ag bulk of different compositions

3.1.1. Energetics and affinities. The positron affinities were first calculated for ordered $Al_{1-x}Ag_x$ alloys as a function of the composition x. For a delocalized positron in a perfect lattice the two-component density functional theory simplifies essentially. Since in this case the positron density is vanishingly small at every point of the infinite lattice it does not influence the electronic structure. The electronic structure of the perfect lattice is therefore first solved by a standard self-consistent band structure code by omitting the positron density and the electron–positron correlation potential. The effective electron potential is

$$v_{eff}(\boldsymbol{r}) = \varphi(\boldsymbol{r}) + v_{xc}(n(\boldsymbol{r})) \tag{1}$$

where $\varphi(\boldsymbol{r})$ is the Coulomb potential due to the nuclei and electron charge density and $v_{xc}(n(\boldsymbol{r}))$ is the LDA exchange–correlation potential, which depends on the electron density $n(\boldsymbol{r})$.

The potential sensed by the positron is

$$V_+(\boldsymbol{r}) = -\varphi(\boldsymbol{r}) + V_{corr}(n(\boldsymbol{r})) \tag{2}$$

where $\varphi(\boldsymbol{r})$ is the Coulomb potential as in equation (1), and $V_{corr}(n(\boldsymbol{r}))$ is the correlation potential describing the energy lowering due to the electron pile-up near the positron. The correlation potential $V_{corr}(n(\boldsymbol{r}))$ is treated within the LDA based on the many-body calculations for a delocalized positron in a homogeneous electron gas [20].

Once the potential sensed by the positron has been obtained, the corresponding Schrödinger equation can be solved by using the same band structure code as for electrons. The solution of the positron wave function is needed only for a single delocalized positron in the system. We are only interested in the positron wave function and the energy eigenvalue in the lowest-energy state, i.e. at the bottom of the lowest positron energy band. This corresponds to the positron momentum $\boldsymbol{p} = 0$, and the positron wave function for this state is s type with respect to the nuclear positions in the lattice.

We calculated the self-consistent electronic structures of the different compositions using the linear-muffin-tin-orbital (LMTO) method within the atomic-spheres approximation (ASA) [14]. The radii of the different atoms were chosen to be equal. In the calculation we have assumed the fcc lattice for the alloy with a lattice constant obtained by linear interpolation from the pure metal lattice constants. The valence electron wave functions were determined scalar relativistically using partial waves up to $l = 2$.

In the LMTO–ASA method the potentials and energy levels are given with respect to the so-called *crystal zero* level, which is defined as the zero of the Coulomb potential due to the nuclei and the electron density of the infinite solid. In the ASA the lattice is divided into spheres centred around the nuclei. The spheres fill the whole space and the electron density and the potentials are approximated to be spherical inside these spheres. In case of fcc and bcc metals all the spheres are identical neutral Wigner–Seitz spheres and therefore the Coulomb potential vanishes just outside the sphere surface. The position of the Fermi level relative to the crystal zero defines the electron chemical potential μ_-. For positrons, the position of the bottom of the lowest-energy band relative to the crystal zero gives the positron chemical potential μ_+.

The positron affinity A_+ is defined as the sum

$$A_+ = \mu_- + \mu_+. \tag{3}$$

The importance of the positron affinity is the fact that the difference in the positron energies between different metals in contact is the difference in their positron affinities [14]. Positrons

Table 2. The electron (μ_-) and positron (μ_+) chemical potentials and the positron affinity (A_+) in $Al_{1-x}Ag_x$ as a function of the composition x.

	μ_- (eV)	μ_+ (eV)	A_+ (eV)
Al	−0.46	−3.90	−4.36
Al_3Ag	−0.45	−3.81	−4.26
AlAg	−0.71	−3.72	−4.43
$AlAg_3$	−1.22	−3.65	−4.87
Ag	−1.78	−3.61	−5.39

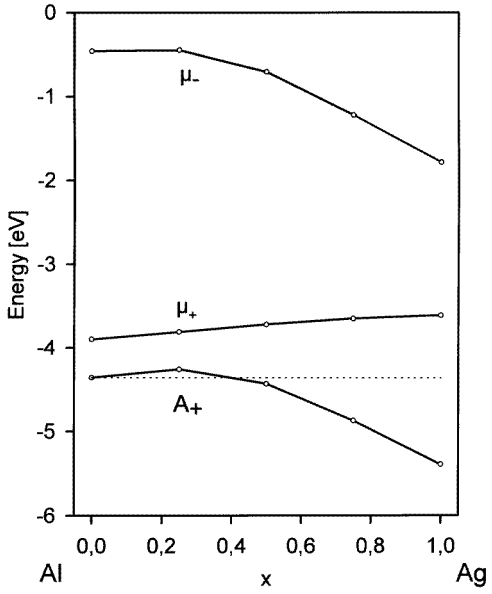

Figure 2. The electron (μ_-) and positron (μ_+) chemical potentials and the positron affinity (A_+) in $Al_{1-x}Ag_x$ as a function of the composition x.

have the lowest energy level in the material whose positron affinity has the largest absolute value.

The calculated chemical potentials and positron affinities are given in table 2 and shown in figure 2. The magnitude of the positron affinity shows a minimum at approximately 25 at.% Ag. The reason for this unexpected result can be found in the nonlinear behaviour of the Fermi energy with varying silver concentration, which has consequences for positron trapping at the GP zones, as discussed below.

3.1.2. Annihilation rates. The positron annihilation rate is proportional to the overlap of positron and electron densities. In the two-component density functional theory formalism [20] the annihilation rate is

$$\lambda = \pi r_0^2 c \int \mathrm{d}\boldsymbol{r}\, n_+(\boldsymbol{r}) n_-(\boldsymbol{r}) g(0; n_+, n_-) \tag{4}$$

where $g(0; n_+, n_-)$ is the electron–positron pair correlation function evaluated at the positron, r_0 the classical electron radius and c the speed of light. As far as only the

positron annihilation rates are considered a non-self-consistent electron density is sufficient. This ensues from the fact that the positron lifetime is determined by the integral over the product of positron and electron densities. The positron density relaxes following electron charge transfer and therefore has the tendency to conserve the value of the overlap integral [21]. This property of the positron annihilation rate enables an efficient and practical method (superimposed atom method [22]) to calculate positron states. It is based on the approximation of the host electron density by the superposition of free atoms. We used this method to calculate the positron annihilation rates and from it the positron lifetimes in Al–Ag as a function of the silver concentration (figure 3). The positron lifetimes for vacancies in aluminium and silver were also calculated. In the lifetime calculations for homogeneously distributed silver atoms a supercell consisting of 32 atoms was used. The positron bulk lifetimes actually used for the predictions of the trapped positron lifetimes in the GP zones are scaled to coincide with the experimentally determined aluminium and silver matrix values. The scaling factor is assumed to be linear in concentration.

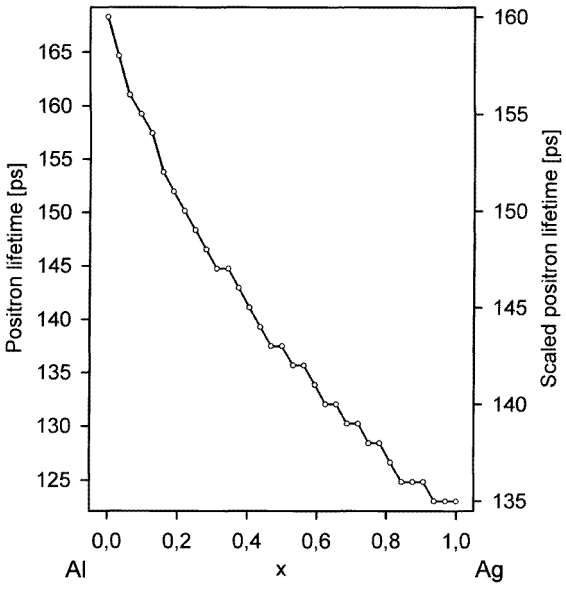

Figure 3. The calculated positron lifetime τ as a function of the silver concentration in Al–Ag. The right scale has been linearily transformed from the left one to obtain agreement with the experimental values for the pure metals.

3.2. Determination of positron annihilation characteristics of GP zones by the method of spherical well potentials

Now the size, structure and composition of the GP zones must be brought in. This is realized in the following way.

(i) Spherical well models are constructed for positrons at GP zones with a given radius r and silver concentration profile. This construction is based on the calculated positron affinities for alloys of different constitution.

(ii) The wave functions (envelope functions) of the positrons trapped in these potentials are calculated.

(iii) The positron lifetimes in the different GP zone models are calculated by weighting the concentration-dependent annihilation rates by the positron probability distribution. The *S*-parameter can also be estimated in this manner.

The positron wave function derived for the spherical well mimicking the GP zone is a pseudo-wave function, enveloping the full wave function, which oscillates with the periodicity of the lattice. Nevertheless it is a proper approximation for the positron distribution, since the envelope function averages over a huge number of atoms and the short-range structure of the wave function is included in the calculated affinity and bulk lifetime. In order to differentiate between the various possible compositions and structures of the GP zones we employed a number of spherically symmetric step potentials, beginning with a simple square well potential to describe the η-particles up to steplike potentials consisting of three different potential depths for the simulation of concentration gradients in ε-particles. A derivation of the solution of the wave function in such a potential (the silver-shell model suggested in [9]) is given in the appendix. The derivations of the solutions for trapped positrons in the other potential models are gained in a similar way.

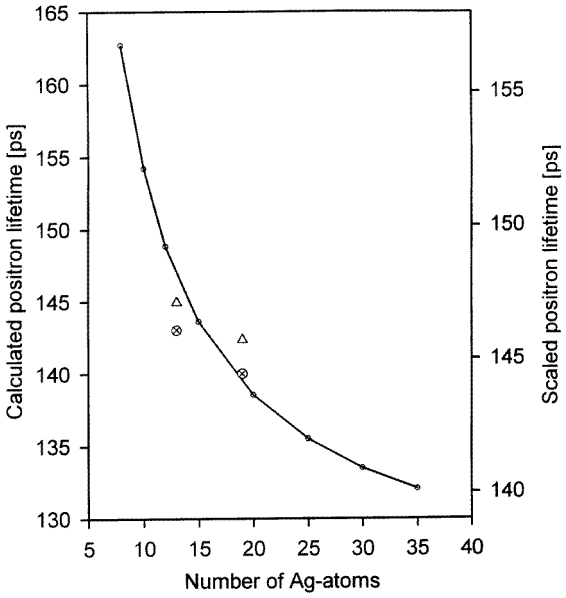

Figure 4. Calculated positron lifetimes in clusters of pure silver. The connected points are calculated with the square-well potential model. ⊗, calculated by Bharathi and Sundar [5]; △, our own superimposed atoms calculations.

In addition, calculations of positron lifetimes for actual silver clusters with various numbers of atoms were performed by using the superimposed atom method, for a quantitative comparison with experiment and for a check of the spherical well methods.

The positron affinity of silver is about one electron volt larger in magnitude than that of aluminium (see figure 2). Therefore the probability function of the positron piles up in the vicinity of silver. It has been shown [14] that for the occurrence of a bound state the critical radius r_c has to be exceeded, which is about 3 Å in the present case. The results of the positron lifetime calculations of small silver clusters in aluminium within the superimposed atoms method and within the square-well potential approximation, which are

shown in figure 4, are in reasonable agreement. For the smallest clusters the lifetime is increased strongly above the Ag value by the considerable overlap of the positron wave function with the matrix.

4. Results and discussion

Trapping of positrons in solid two-phase alloys may occur at particles of a phase which is associated with a potential attractive for positrons or alternatively at defects with reduced ionic and electron density such as vacancies or dislocations. The phase boundaries of particles formed in decomposed alloys may also act as positron traps [23]. Positrons may become localized there at misfit dislocations or at the incoherent particle–matrix interface. In all cases of defects the positron lifetime lies above that of the matrix. As we found in each sample only one lifetime which is *reduced* in comparison with the matrix material (table 1) no influence of defects is visible as has to be expected for coherent interfaces of GP zones.

As we have direct evidence of a marked difference in micro-Vickers hardness between samples containing ε- and η-zones there must be a structural difference between the respective samples. A higher particle density due to nucleation at higher supersaturation for the lower annealing temperatures can be ruled out because the hardness change turns out to be reversible if the temperature is cycled between 190 and 150 °C. Assuming that different particles dominate the two temperature regions (η-zones at 150 °C and ε-zones at 190 °C) the difference in the structure of these precipitates has to be responsible for the hardness change.

In all our experiments we find a single positron lifetime, which undoubtedly arises from trapping at GP zones. Even for the RT-annealed samples the occurrence of small silver clusters (of about ten atoms or less) is ruled out by the lifetimes measured (compare table 1 and figure 4). Furthermore we obtain no significant difference between lifetimes and S-parameters for η- and ε-particles in 1 and 6 at.% Ag alloys (see table 1).

From the fact that ε-particles trap positrons and from the values of the annihilation parameters (table 1) we can deduce information about their structure and concentration by careful comparison with suitable model calculations for the structures in discussion.

Particles with less than 45 at.% Ag distributed homogeneously would not trap positrons as can be concluded from the calculated positron affinities given in table 2 and figure 2. The calculation shows that a linear interpolation for positron affinities of Al and Ag is considerably in error due to the specific behaviour of the Fermi energy (electron chemical potential μ_-) having led to wrong conclusions in the past [6, 7]. The occurrence of trapping excludes all structures of homogeneously distributed Ag atoms with less than 45 at.% concentration. Thus the possibility of a strongly asymmetrical miscibility gap can be ruled out.

For a check of the validity of a multi-phase model with strongly inhomogeneous distribution of the Ag atoms inside the ε-GP zones we worked out three different spherical step potentials:

(i) according to the Dubey model [18], a silver-depleted core decorated with a shell of pure silver;

(ii) a silver core surrounded by a silver-depleted shell corresponding to the model of Naudon and Caisso [8];

(iii) an aluminium core surrounded by increasing Ag concentration simulated by three regions of constant concentration.

Table 3. Calculated positron lifetimes and *S*-parameters in the two-shell model. r_1 is the core radius, r_2 the radius of the particle. The shell widths are interpolated by using the conservation of the atomic number in the precipitate.

r_2 (Å)	r_1 (Å)	τ (ps)	S/S_{Al}	Core at.% Ag	Shell at.% Ag	Total at.% Ag
20	16	140.5	0.9060	30	100	66
25	21	138.8	0.8959	30	100	66
70	56	135.4	0.8738	30	100	66
20	16	150.3	0.9615	15	66	33
25	21	149.7	0.9614	15	66	33
70	56	143.8	0.9279	15	66	33

The results of configuration (i) for three different particle sizes are presented in table 3. In the upper half the overall silver concentration of the precipitate is assumed to be 66 at.%, which is the concentration of the successor particles γ and γ'. The smallest particle radii must be about 20 Å, since otherwise a coating of pure silver cannot build up by transformation of η-zones. The silver content of the core is supposed to be 30 at.% [9]. The most characteristic feature is the marked dependence of the positron lifetime on particle diameter, which is not found in our experiments, where ε-particles with radii between 20 and 30 Å have been produced during the 190 °C annealings and considerably larger ε-particles with stepwise quenching. Thus the model of ε-particles with pure silver coating does not agree with our results. The correspondence of the lifetime obtained for $r = 20$ Å with the experiment seems to be fortuitous. A possibility for trapping in the case of an overall concentration of 33 at.% Ag and a silver-depleted core is also shown in table 3. The calculated positron lifetimes are definitely too long for small and medium-sized particles. Only particles with radii of about 70 Å would be in agreement with our measurements.

As an example for configuration (ii) a precipitate of radius 25 Å and an overall concentration of 66 at.% Ag is considered. For a core radius of 17 Å and a silver concentration of 33 at.% for the remaining particle, the positron wave function is nearly completely confined within the core region and the lifetime is that of pure silver. It becomes apparent that the configuration (ii) gives the same positron lifetimes as the simple silver cluster model; these are situated far below the values determined in our experiment for particles of this size.

The situation for model (iii) is very similar to that for (i). Again there is a radius dependence of lifetime in contradiction to experiment and also trapping at an overall concentration of 33 at.% can occur. For a silver content above 60 at.% the silver gradient model results in positron lifetimes too short to be compatible with our experimental results (see tables 3 and 4).

Thus we have shown that no multi-phase model is in agreement with the experimental positron lifetimes. Therefore the only possibility is a homogeneous distribution of the silver atoms inside the ε-particle.

For homogeneously distributed silver inside the GP zones the silver concentration is determined by using the spherical well model with experimentally obtained radii for a homogeneous silver distribution and different concentrations. The calculated and calibrated lifetimes (see section 3) can be compared with the experimentally determined lifetimes of the trapped positrons. In figure 5 the calculated positron lifetimes are shown as a function of the particle radius for different concentrations. It can be seen that a strong radius dependence exists for particles only slightly larger than the critical radius for trapping,

Table 4. Calculated positron lifetimes in the ε-GP zone with a gradual change in silver concentration (three-shell model).

r_3 (Å)	r_2 (Å)	r_1 (Å)	τ (ps)	S/S_{Al}	Core at.% Ag	Shell1 at.% Ag	Shell2 at.% Ag	Total at.% Ag
25	21	18	150.2	0.9614	0	33	66	33
20	16	13.2	140	0.9032	0	50	100	60
25	21	14.8	139.6	0.9008	0	50	100	60
30	25	18	138.4	0.8932	0	50	100	60

which is about 8 Å in this case. This is due to an increasing overlap of the positron wave function with the matrix. A corresponding change of positron lifetime and *S*-parameter is indeed experimentally observed between the 1 at.% Ag samples, where precipitates are about 10 Å in radius and the 6 at.% Ag samples, where they are considerably larger. The experimental lifetimes are inserted in figure 5 and indicate that the silver concentrations inside the particles are identical in both cases. We obtain a concentration of 60 ± 5 at.% Ag.

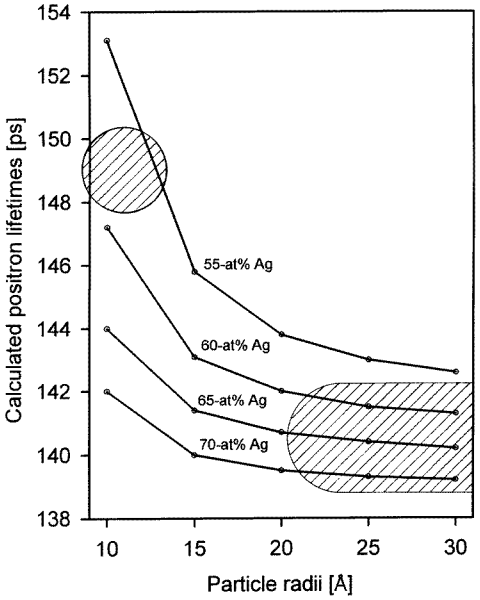

Figure 5. Calculated positron lifetimes from the square-well model for four different silver concentrations and five different radii. The shaded areas indicate our lifetime measurement results allowing for experimental uncertainties.

Thus we find no significant difference in silver concentration of the different types of GP zone and no shoulder in the miscibility gap of the phase diagram. There are also no hints of an internal structure in the ε-particles. This is in contradiction with the results of Dlubek and Krause [4, 6, 7], who conclude from their measurements a decrease of the silver concentration in ε-GP zones down to about 35 at.%. The rise of the lifetime and *S*-parameter with increasing temperatures in their *in situ* experiments can be possibly explained by thermal detrapping (see [24]) in the case of shallow trapping potentials. In particles

with a homogeneous silver concentration in the vicinity of 55 at.% (binding energy about −0.13 eV) the annihilation parameters should increase about 5% from RT up to 200 °C.

As an explanation for the abrupt and reversible change of various physical parameters (hardness, electrical resistivity) around 170 °C, which is as well in agreement with our investigation as with the results discussed in the introduction, there remains the possibility that η-precipitates are short-range ordered [3, 10], while the ε-precipitates are disordered, but of the same silver concentration.

5. Summary

From comparison of experimental PAS data with careful calculations of positron affinities and lifetimes of different structures of precipitates we conclude that

(i) ε-zones cannot be described by any of the multi-phase models proposed,
(ii) the Ag concentration of the η-particles and the ε-particles is 60 ± 5 at.%,
(iii) no asymmetry in the miscibility gap of the phase diagram occurs and
(iv) an order–disorder transformation from η- to ε-particles would be in agreement with the positron data.

The importance of careful calculations of positron affinity and annihilation parameters for the interpretation of experimental PAS data has to be emphasized.

Acknowledgments

One of us (GB) would like to thank the positron group of the Helsinki University of Technology for warm hospitality and in particular M Puska for his help and advice in learning to carry out the first-principles calculations. Furthermore we are indebted to R Podloucky for valuable discussions, T Ntaflos for the microprobe investigations and F Langmayr for the SAXS measurements. The work was supported by the FWF grant No S 5603 and by the University of Vienna.

Appendix. Spherical well model for precipitates

For a proper interpretation of the experimentally derived PAS data we need a tractable model for the description of the behaviour of the trapped positrons in all the possible internal structures of the precipitates. Therefore we employ three-dimensional spherical square-well-type potentials. The depths are taken as the difference ΔA_+ of the positron affinities between the particular region of the precipitate and the bulk.

For spherically symmetric systems we can consider the potential

$$V(r) = \begin{cases} V_1 & 0 \leqslant r < r_1 \ldots q = 1 \\ V_2 & r_1 \leqslant r < r_2 \ldots q = 2 \\ \vdots & \vdots \\ V_N & r_{N-1} \leqslant r \ldots q = N. \end{cases} \tag{A1}$$

The radial wave function $R_{nl}(r)$ to the energy eigenvalue E_{nl} consists of N parts R_{nlq}, where each part satisfies the radial Schrödinger equation

$$\left(-\frac{\hbar^2}{2m} \frac{1}{r} \frac{\mathrm{d}^2}{\mathrm{d}r^2} r + \frac{l(l+1)\hbar^2}{2mr^2} \right) R_{nlq}(r) = (E_{nl} - V_q) R_{nlq}(r). \tag{A2}$$

The bound state solutions occur for discrete values of negative energies E. The R_{nlq} are linear combinations of spherical Bessel and Neumann functions in regions with $E_{nl} > V_q$ and a linear combination of Hankel functions in regions with $E_{nl} < V_q$ (see e.g. [25]). The continuity of the wave functions and their derivatives at the boundaries provide $2(N-1)$ conditions for $2N-2$ coefficients. For each angular momentum l this gives a system of $2N-2$ linear equations for the same number of unknowns. There exists a nontrivial solution if the determinant $D_l = D_l(E)$ vanishes. From this follows a transcendental equation for the energy eigenvalue E_{nl}:

$$D_l(E_{nl}) = 0. \tag{A3}$$

After determining the eigenvalue E_{nl} as a single root of (A3) the system of linear equations resulting from the boundary conditions can be solved and the coefficients can be determined with the normalizing condition

$$\int_0^\infty R_{nl}^*(r) R_{nl}(r) r^2 \,\mathrm{d}r = 1. \tag{A4}$$

We used four different square-well potentials to approximate the various possible internal structures of the GP zones. As an example of the models the solution for the ε-particles with a silver-depleted core and a pure silver coating is elaborated.

In order to find the envelope function of the trapped positron wave function in the ε-GP zone, we match the following solutions (see figure A1):

$$\begin{array}{llll}
\text{core(c):}\ E < V_1 & \kappa_1 = \sqrt{2m(V_1 - E)}/\hbar & R_c(r) = A\sin(\kappa_1 r)/\kappa_1 r \\
\text{shell(s):}\ E > V_2 & k = \sqrt{2m(E - V_2)}/\hbar & R_s(r) = B\sin(kr)/kr + C\cos(kr)/kr \\
\text{bulk(b):}\ E < V_0 (= 0) & \kappa = \sqrt{2m(-E)}/\hbar & R_b(r) = D\mathrm{e}^{-\kappa r}/\mathrm{i}\kappa r.
\end{array} \tag{A5}$$

Since the trapped positrons are for the most part in the ground state, only the states for $l = 0$ are regarded. We introduce the abbreviations

$$\alpha = \sinh(\kappa_1 r)/\kappa_1 r \qquad \beta = \sin(kr)/kr \qquad \gamma = \cos(kr)/kr \qquad \delta = \mathrm{e}^{-\kappa r}/\mathrm{i}\kappa r \tag{A6}$$

and obtain a system of linear equations which has nontrivial solutions only if its determinant vanishes:

$$\begin{vmatrix}
\alpha(r_1) & -\beta(r_1) & -\gamma(r_1) & 0 \\
\dfrac{\partial}{\partial r}\alpha(r_1) & -\dfrac{\partial}{\partial r}\beta(r_1) & -\dfrac{\partial}{\partial r}\gamma(r_1) & 0 \\
0 & \beta(r_2) & \gamma(r_2) & -\delta(r_2) \\
0 & \dfrac{\partial}{\partial r}\beta(r_2) & \dfrac{\partial}{\partial r}\gamma(r_2) & -\dfrac{\partial}{\partial r}\delta(r_2)
\end{vmatrix} = 0. \tag{A7}$$

After the solution of (A7) and some simple transformations the eigenvalue equation for the energy of the positron trapped in the GP zone is obtained:

$$\frac{\tan(kr_1) - (k/\kappa_1)\tanh(\kappa_1 r_1)}{1 + (k/\kappa_1)\tanh(\kappa_1 r_1)\tan(kr_1)} = \frac{(\kappa/k)\tan(kr_2) + 1}{(\kappa/k) - \tan(kr_2)}. \tag{A8}$$

(A8) is solved numerically and as a consequence of this the coefficients B, C and D can be calculated in terms of A. The remaining coefficient A follows from the normalization of the wave function (A4).

The square of the wave function represents the probability density of the positron in the respective regions of the precipitate and can therefore be used for weighting the positron lifetimes in the core, shell and bulk regions:

$$\lambda_\varepsilon = \int_0^{r_1} |R_i(r)|^2 r^2 \,\mathrm{d}r\, \lambda_c + \int_{r_1}^{r_2} |R_{ii}(r)|^2 r^2 \,\mathrm{d}r\, \lambda_s + \int_{r_2}^{\infty} |R_{iii}(r)|^2 r^2 \,\mathrm{d}r\, \lambda_b \tag{A9}$$

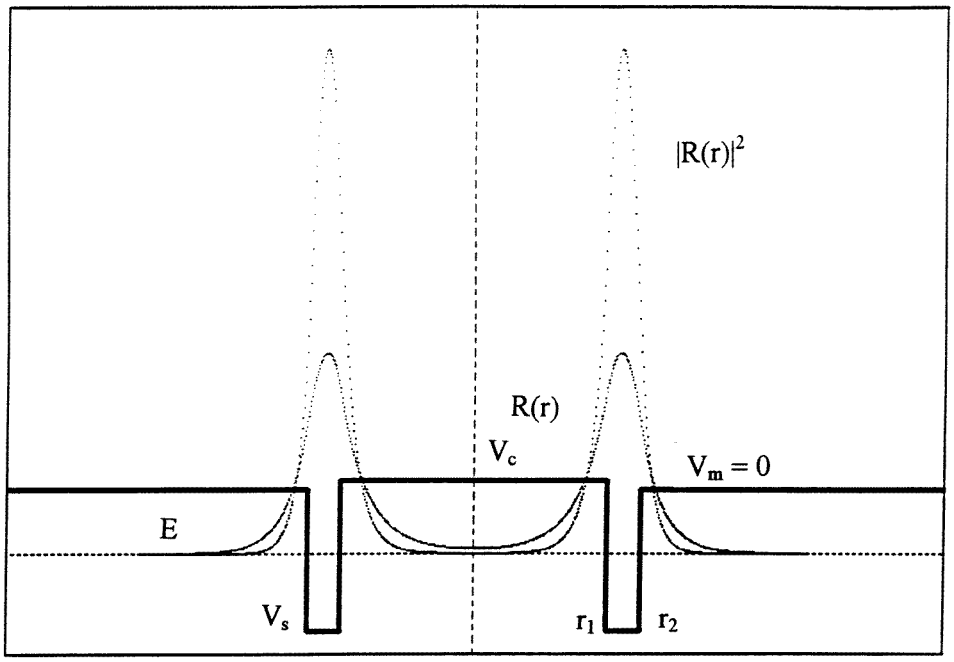

Figure A1. The three-dimensional spherical square-well potential of the ε-GP zone with a shell of pure silver.

where the λ_i are the numerically determined positron annihilation rates in Al–Ag with the homogeneous silver concentration of the bulk (λ_b), the shell (λ_s) and the core region (λ_c).

Now there arises the question of the minimum thickness of the silver shell in order to allow positron trapping. A simple estimate is the limit of vanishing positron energy ($E \rightarrow 0$) in the eigenvalue equation (A8). It turns out that for particles with radii of about 20 Å a monoatomic layer of silver atoms would be sufficient for positron trapping.

References

[1] Köster W and Braumann F 1952 *Z. Metallk.* **43** 193
Köster W, Steinert H and Schreb J 1952 *Z. Metallk.* **43** 202
[2] Baur R and Gerold V 1962 *Acta Metall.* **10** 637
[3] Osamura K, Nakamura T, Kobayashi A, Hashizume T and Sakurai T 1987 *Scr. Metall.* **21** 255
[4] Krause R, Dlubek G, Wendrock G and Brümmer O 1986 *Scr. Metall.* **20** 1761
[5] Bharathi A and Sundar C A 1988 *Positron Annihilation Proc. 8th Int. Conf. (Gent)* ed L Dorikens-Vanpraet, M Dorikens and D Segers (Singapore: World Scientific) p 479
[6] Dlubek G, Unger R, Pawelzyk K, Gläser U H and Wendrock G 1992 *Mater. Sci. Forum* **105–110** 981
[7] Dlubek G, Wendrock G and Pawelzyk K 1993 *Phys. Status Solidi* a **140** 311
[8] Naudon A and Caisso J 1974 *J. Appl. Crystallogr.* **7** 25
[9] Dubey Ph A, Schönfeld B and Kostorz G 1991 *Acta Metall. Mater.* **39** 1161
[10] Auer H and Gerold V 1965 *Z. Metallk.* **56** 240
[11] Ernst F and Haasen P 1987 *Phys. Status Solidi* a **104** 403
[12] Al-Kassab T and Haasen P 1993 *Z. Metallk.* **84** 248
[13] Langmayr F, Fratzl P and Vogl G 1992 *Acta Metall. Mater.* **40** 3381
[14] Puska M J, Lanki P and Nieminen R M 1989 *J. Phys.: Condens. Matter* **1** 6081
[15] Kirkegaard P and Eldrup M 1974 *Comput. Phys. Commun.* **7** 401

[16] Kirkegaard P, Eldrup M, Mogensen O E and Pedersen N J 1981 *Comput. Phys. Commun.* **23** 307
[17] Campbell J L 1977 *Appl. Phys.* **13** 365
[18] Dubey Ph A 1990 *Dr. Sc. Nat. Dissertation* **9077** ETH Zürich
[19] Puska M J and Nieminen R M 1994 *Rev. Mod. Phys.* **66** 3
[20] Boronski E and Nieminen R M 1986 *Phys. Rev.* B **34** 3820
[21] Puska M J 1983 *Phys. Status Solidi* a **102** 11
[22] Puska M J and Nieminen R M 1983 *J. Phys. F: Met. Phys.* **13** 333
[23] Gröger V, Fratzl P, Pahl W, Paris O, Bischof G and Krexner G 1995 *Acta Metall. Mater.* **43** 1305
[24] Manninen M and Nieminen R M 1981 *Appl. Phys.* A **26** 93
[25] Brandt S and Paulin R 1985 *The Picture Book of Quantum Mechanics* (New York: Wiley)
[26] Borelius G 1955 *Defects in Crystalline Solids* (London: Physical Society) p 169